

Mesons at finite baryon density in $(2+1)d$

Costas G. STROUTHOS

Department of Physics, Duke University, Durham, NC 27708-0305, USA

We discuss the critical properties of the three-dimensional Gross-Neveu model at nonzero temperature and nonzero chemical potential. We also present numerical and analytical results for the in-medium interaction due to scalar meson exchange. Further, we discuss in-medium modifications of mesonic dispersion relations and wavefunctions.

§1. Introduction

Chiral phase transitions and the spectrum of excitations in strongly interacting matter at finite baryon chemical potential remain interesting challenges. Strongly interacting systems are intrinsically non-perturbative and therefore most of our knowledge about the relevant phenomena comes from lattice simulations. Unfortunately, the complex nature of the determinant of the QCD Dirac operator at finite chemical potential makes it impossible to use standard simulation techniques to study Fermi surface phenomena in Euclidean simulations.

In order to understand what ingredients might play a decisive role in more complex systems such as gauge theories, we have studied the simplest non-trivial model simulable with $\mu \neq 0$ using standard algorithms, namely the three-dimensional Gross-Neveu model (GNM₃). Its Lagrangian in Euclidean metric is written in terms of $4N_f$ -component spinors $\psi, \bar{\psi}$ as

$$\mathcal{L} = \bar{\psi}(\partial + m)\psi - \frac{g^2}{2N_f}(\bar{\psi}\psi)^2. \quad (1.1)$$

In the chiral limit $m = 0$ the model has a global Z₂ symmetry $\psi \mapsto \gamma_5\psi, \bar{\psi} \mapsto -\bar{\psi}\gamma_5$. At tree level, the fields σ and π have no dynamics; they are truly auxiliary fields. However, they acquire dynamical content by dint of quantum effects arising from integrating out the fermions. The model is renormalizable in the $1/N_f$ expansion unlike in the loop expansion.¹⁾ Apart from the obvious numerical advantages of working with a relatively simple model there are several other motivations for studying this model. At $T = \mu = 0$ for sufficiently strong coupling g^2 , the chiral symmetry is spontaneously broken by a condensate $\langle \bar{\psi}\psi \rangle \neq 0$ leading to a dynamically generated fermion mass gap given by $M_f = g^2\langle \bar{\psi}\psi \rangle \gg m$ in the large- N_f approximation. The spectrum of excitations contains both baryons and mesons, i.e. the elementary fermions f and the composite $f\bar{f}$ states. The critical coupling g_c^2 at which the gap $M_f/\Lambda_{UV} \rightarrow 0$, defines an ultra-violet stable fixed point of the renormalisation group at which an interacting continuum limit may be taken. This picture has been verified both at next-to-leading order in $1/N_f$ and by Monte Carlo simulations with finite N_f .²⁾

In the next sections we will discuss chiral symmetry restoration at nonzero

fermion chemical potential. Then we will discuss Fermi surface phenomena, such as long range interparticle interaction in medium. We will also present results for dispersion relations and wavefunctions of massless particle-hole excitations on or near the Fermi surface. A study of the dispersion relation of spin- $\frac{1}{2}$ excitations around the Fermi surface has shown that there is no mass gap characteristic of a BCS instability³⁾ and the values of the Fermi liquid parameters (Fermi momentum, Fermi velocity) are in good agreement with the $1/N_f$ predictions. However, in a different study of a related model, the $(2+1)d$ NJL model, which has an $SU(2) \otimes SU(2)$ chiral symmetry, it was shown that although the BCS instability is also absent the properties of the quasi-particle spectrum is determined by physics outside the scope of the $1/N_f$ expansion.⁴⁾

§2. Chiral phase transitions

The action of the NJL model remains real even after the introduction of nonzero chemical potential μ , which means we can study the physics of the high density regime using standard Monte Carlo techniques. In the presence of a Fermi surface with Fermi momentum p_F the creation of $f\bar{f}$ pairs with zero net momentum is energetically suppressed, because one can only create particles with $p > p_F$. So as the fermion number density $\eta(\mu)$ grows the chiral symmetry breaking is suppressed. The large- N_f description of the $\mu \neq 0$ chiral phase transition predicts a first order transition for $T = 0$ and a continuous transition for $T > 0$.⁵⁾ Furthermore, the critical value of the chemical potential μ_c is equal to the value of the fermion mass at $\mu = 0$, which indicates that materialization of the fermion itself drives the symmetry restoration transition. Interactions as expected decrease μ_c below the mean field result.⁶⁾ Work by Stephanov⁷⁾ suggests that any non-zero density simulation which incorporates a real path integral measure proportional to $\det(MM^\dagger)$ is doomed to failure due to the formation of a light baryonic pion from a quark q and a conjugate quark q^c . The NJL model however, does not exhibit such a pathology, because the realization of the Goldstone mechanism in this model is fundamentally different from that in QCD. In the NJL model the Goldstone mechanism is realized by a pseudoscalar channel pole formed from disconnected diagrams and the connected diagrams yield a bound state of mass $\approx 2m_f$.⁸⁾ This implies the absence of a light qq^c state.

As expected our simulations of GNM₃ with $N_f = 4$ ⁹⁾ did not provide any evidence for the existence of a nuclear liquid-gas transition at $\mu < \mu_c$. It was shown in¹⁰⁾ that in the standard four-fermi models there is no saturation density for stable matter. In order to get the saturation features the authors of¹⁰⁾ introduced a chirally invariant scalar-vector interaction term which cures the binding problem. Furthermore, our results showed that the second order nature of the $T \neq 0, \mu = 0$ transition remains stable down to low T and large μ . In Fig.1 (left) we plot the normalized order parameter $\Sigma(T, \mu)/\Sigma(T, 0)$ ($\Sigma \equiv \langle \sigma \rangle$) as a function of μ/m_f at different values of T . It is clear from the shapes of these curves that the transition becomes sharper as we decrease the temperature. In Fig.1 (right) we plot the normalized fermion number density as a function of the chemical potential at different values

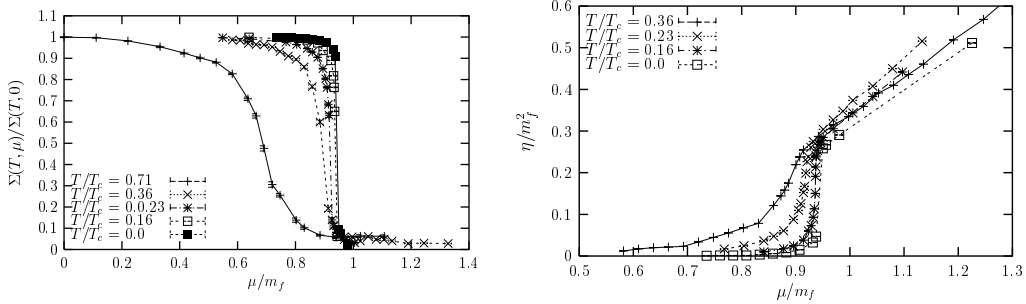


Fig. 1. Chiral order parameter (left) and fermion number density (right) vs. chemical potential at various values of T .

of T . In the limit $T \rightarrow 0$ we see that the fermion density is strongly suppressed before the transition and then jumps discontinuously. By performing detailed finite size scaling analysis which allowed us to distinguish between second order and weak first order transitions we showed that the tricritical point lies on the section of the phase boundary defined by $T/T_c \leq 0.23$, $\mu/\mu_c \geq 0.97$.⁹⁾ It was also shown some time ago¹¹⁾ that the second order transitions belong to the $2d$ Ising universality class in accordance with the dimensional reduction scenario.

§3. The sigma propagator in medium

In this section we examine the auxiliary scalar propagator D_σ in the presence of non-zero baryon density. Although at tree level σ is non-propagating, the leading order $1/N_f$ expansion at $\mu = 0$ predicts that it acquires dynamics through quantum corrections due to virtual $q\bar{q}$ pairs, resulting in a propagator of the form^{1), 2)}

$$D_\sigma(k^2) = \frac{1}{g^2} \frac{(4\pi)^{\frac{d}{2}}}{2\Gamma(2 - \frac{d}{2})} \frac{M_f^{4-d}}{(k^2 + 4M_f^2)F(1, 2 - \frac{d}{2}; \frac{3}{2}; -\frac{k^2}{4M_f^2})}. \quad (3.1)$$

Immediately we see the difference between this model and QCD. For $k^2 \ll M_f^2$ the hypergeometric function $F \approx 1$, implying that to this order the σ resembles a weakly-bound meson of mass $M_\sigma = 2M_f$; however, the hypergeometric function in the denominator indicates a strongly interacting $q\bar{q}$ continuum immediately above the threshold $2M_f$. This implies that if truly bound, its binding energy is $O(1/N_f)$ at best (to our knowledge there have so far been no analytic calculations), implying little if any separation between pole and threshold. A recent study using the maximum entropy method has shown evidence for a nonzero binding energy in the σ channel for finite $N_f = 4$.¹²⁾ Since all residual interactions are subleading in $1/N_f$, we surmise that all other mesons are similarly weakly bound states of massive fermions, and hence effectively described by a two-dimensional “non-relativistic quark model”.

Similarly, at nonzero chemical potential μ to leading order in the $1/N_f$ expansion, we have

$$D_\sigma^{-1}(k) = 1 - \Pi(k; \mu)$$

$$= g^2 \left[\frac{1}{\Sigma_0} \int_{q,\mu=0} \text{tr} \frac{1}{i\cancel{q} + \Sigma_0} + \int_{q,\mu>\mu_c} \text{tr} \frac{1}{i\cancel{q} + \mu\gamma_0} \frac{1}{i(\cancel{q} - \cancel{k}) + \mu\gamma_0} \right], \quad (3.2)$$

where Π is the virtual fermion-antifermion vacuum polarization bubble. We have used the gap equation at $\mu = 0$ to express $1/g^2$ in terms of the zero density gap Σ_0 and assumed that the gap vanished in the integral defining Π for $\mu > \mu_c$. The functional form of the propagator in the Hard Dense Loop (HDL) approximation ($k_0, |\vec{k}| \ll \mu$) in $d+1$ dimensions is given by³

$$D_\sigma^{-1}(k_0, \vec{k}) = \frac{g^2 \mu^{d-3}}{(4\pi)^{\frac{d}{2}} \Gamma(\frac{d}{2})(3-d)} \left[4 \frac{(3-d)}{(d-1)} \mu^{3-d} (\mu^{d-1} - \mu_c^{d-1}) + k_0^2 + |\vec{k}|^2 \left(1 - \frac{(3-d)(k_0^2 + |\vec{k}|^2)^{\frac{1}{2}}}{k_0 + (k_0^2 + |\vec{k}|^2)^{\frac{1}{2}}} \right) + i \frac{k_0 |\vec{k}|^2}{4\mu} \left(1 + \frac{|\vec{k}|^2}{[k_0 + (k_0^2 + |\vec{k}|^2)^{\frac{1}{2}}]^2} \right) + O\left(\frac{k^4}{\mu^2}\right) \right]. \quad (3.3)$$

An interesting observation is that in the static limit $k_0 = 0$ the momentum dependence of eq. (3.4) vanished for the value $d = 2$ implying complete screening for the static potential due to σ exchange. Furthermore, for $\vec{k} = \vec{0}$ D_σ is proportional to a conventional zero-momentum boson propagator with mass

$$M_\sigma = 2\sqrt{\mu(\mu - \mu_c)}, \quad (3.4)$$

implying that just above the transition there is a tightly bound state. In Fig. 2 we show the results for the sigma correlator obtained from numerical simulations with $N_f = 4$ and $1/g^2 = 0.75$ on 48×32^2 lattices. The value of the critical chemical potential $\mu_c = 0.17(1)$. The numerical results for M_σ fall 20 – 30% lower than the

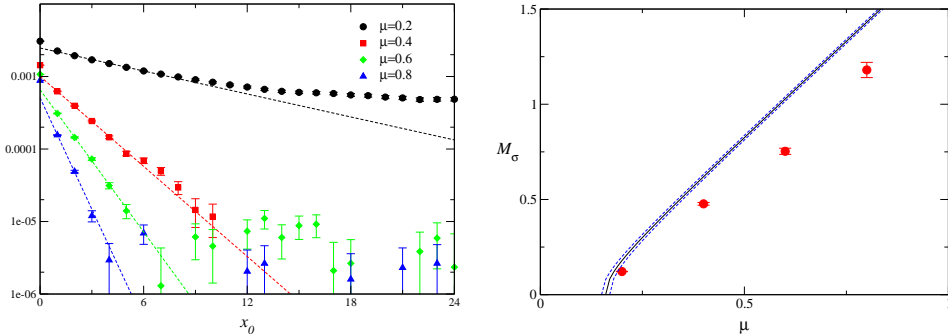


Fig. 2. The zero momentum σ timeslice correlator for 4 values of μ (left) and the M_σ as a function of μ (right). The line is the leading order $1/N_f$ prediction.

leading order prediction, which is consistent with a correction of $O(N_f^{-1})$.

§4. Mesonic dispersion relations

In this section we investigate mesonic states by measuring the connected contribution to the correlation functions $\mathcal{C}_\Gamma(\vec{k}, x_0) = \sum_{\vec{x}} \langle j_\Gamma(\vec{0}, 0) j_\Gamma^\dagger(\vec{x}, x_0) \rangle e^{-i\vec{k} \cdot \vec{x}}$ where

the bilinears $j_\Gamma(x)$ are defined with scalar, pseudoscalar or vector quantum numbers. In terms of staggered fermion fields $\chi, \bar{\chi}$ the operators are

$$j_1(x) = \bar{\chi}_x \chi_x; \quad j_{\gamma_5}(x) = \varepsilon_x \bar{\chi}_x \chi_x; \quad j_{\gamma_i}(x) = \frac{\eta_{ix}}{2} [\bar{\chi}_x \chi_{x+i} + \bar{\chi}_{x+i} \chi_x], \quad (4.1)$$

where $\eta_{1x} = (-1)^{x_0}$, $\eta_{2x} = (-1)^{x_0+x_1}$ and $\varepsilon_x = (-1)^{x_0+x_1+x_2}$. As before we study the timeslice correlators in each channel as a function of spatial momentum $\vec{k} \parallel \hat{x}$.

It was shown³⁾ that in free field theory for $\mu > \mu_c$ the function the $x_0 \rightarrow 0$ limit

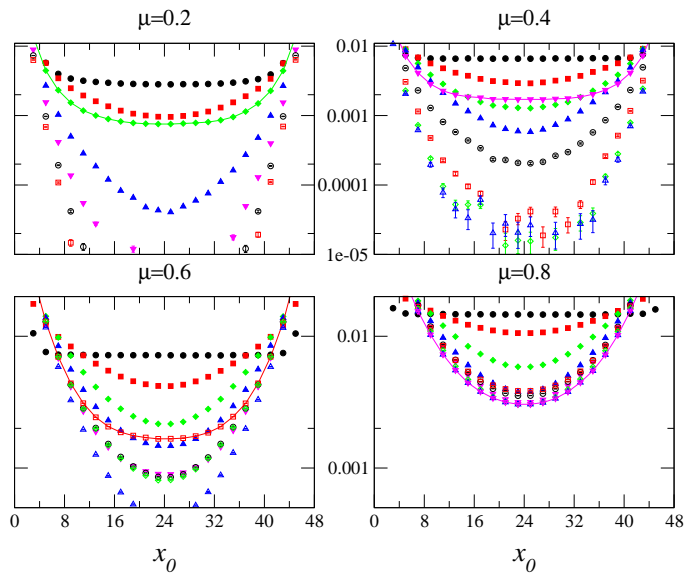


Fig. 3. Pseudoscalar correlator $\mathcal{C}_{\gamma_5}(|\vec{k}|, x_0)$ at 4 different μ for momenta $|\vec{k}| = 0$ (filled circles), $\frac{\pi}{16}$ (filled squares), $\frac{\pi}{8}$ (filled diamonds), $\frac{3\pi}{16}$ (filled up triangles), $\frac{\pi}{4}$ (filled down triangles), $\frac{5\pi}{16}$ (open circles), $\frac{3\pi}{8}$ (open squares), $\frac{7\pi}{16}$ (open diamonds) and $\frac{\pi}{2}$ (open up triangles).

$\mathcal{C}_\Gamma(\vec{k}, x_0)$ is dominated by a continuum of particle-hole pairs at or near the Fermi surface, which effectively cost zero energy to excite. The generic result is that for $|\vec{k}| \leq 2\mu$ the decay is algebraic, with

$$\mathcal{C}_\Gamma(\vec{k}, x_0) \propto \begin{cases} x_0^{-2} & |\vec{k}| \ll \mu; \\ x_0^{-\frac{3}{2}} & |\vec{k}| \simeq 2\mu. \end{cases} \quad (4.2)$$

Only once $|\vec{k}| > 2\mu$ does it become kinematically impossible to excite a pair with zero energy, resulting in exponential decay:

$$\mathcal{C}_\Gamma(\vec{k}, x_0) \propto x_0^{-\frac{3}{2}} \exp\left(-(|\vec{k}| - 2\mu)x_0\right). \quad (4.3)$$

The sequence of plots in Fig. 3 is in qualitative agreement with these findings. For each μ there is a particular value of $|\vec{k}|$, highlighted with a solid line in the plots, for which the temporal falloff is particularly slow, corresponding to $|\vec{k}| \approx 2\mu$ (e.g. for

$\mu = 0.4$ the slow falloff occurs for $|\vec{k}| = \frac{\pi}{4} \simeq 0.785$). For $|\vec{k}|$ larger than this value the decay is much steeper, although only for $\mu = 0.2$ does it resemble an exponential form. Because of the technical difficulties in treating correlators with power-law decays in a finite volume we have made no attempt to fit the numerical data for $\mathcal{C}_{\gamma_5}(|\vec{k}|, x_0)$ to a functional form.

Light states in the ρ channel have long been of interest. Here we discuss tentative results in the vector channel, corresponding to the quantum numbers of the ρ meson. In this case for $|\vec{k}| > 0$ we can distinguish between $\mathcal{C}_{\gamma_{\parallel}}(\vec{k})$, in which the component of the vector is parallel to \vec{k} , and $\mathcal{C}_{\gamma_{\perp}}(\vec{k})$. In Fig. 4 we plot the correlator for several $|\vec{k}|$ values at $\mu = 0.6$ in each case. For $\mathcal{C}_{\gamma_{\perp}}$ the curves are qualitatively very similar to those of Fig. 3 at $\mu = 0.6$, with a distinguished momentum $|\vec{k}| = \frac{3\pi}{8}$. The correlator $\mathcal{C}_{\gamma_{\parallel}}$ is much smaller in magnitude, and is consistent with exponential rather than algebraic decay. The lines are fits of the form $\mathcal{C}_{\gamma_{\parallel}}(|\vec{k}|, x_0) = A(e^{-Ex_0} + e^{-E(L_t - x_0)})$. For small $|\vec{k}|$ the resulting $E(|\vec{k}|)$ resembles that of a massless pole, ie. $E = \beta_0|\vec{k}|$, with velocity $\beta_0 \approx 0.5$. It should be mentioned, however, that although $\mathcal{C}_{\gamma_{\parallel}}$ and $\mathcal{C}_{\gamma_{\perp}}$ still differed, no evidence for a massless pole was seen in the data at $\mu = 0.8$. A potential problem for this picture is that the extracted velocity $\beta_0 \approx 0.5$ is less than $\beta_F \approx 1$, implying that quasiparticles would experience damping via Čerenkov radiation of zero sound. Clearly further work exploring the systematic effects of varying μ , g^2 , \vec{k} and volume will be needed for a more complete understanding to emerge.

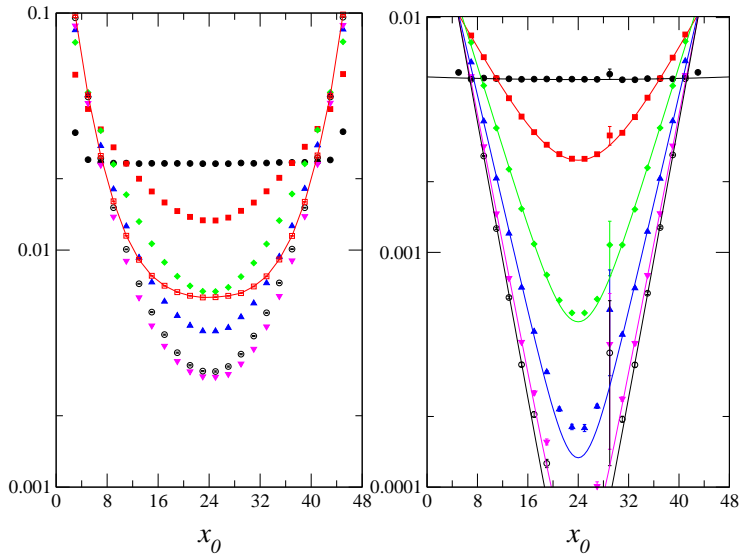


Fig. 4. Vector correlators $\mathcal{C}_{\gamma_{\perp}}(|\vec{k}|, x_0)$ (left) and $\mathcal{C}_{\gamma_{\parallel}}(\pi - |\vec{k}|, x_0)$ (right) at $\mu = 0.6$. The symbols have the same meaning as in Fig. 3.

§5. Mesonic wavefunctions and Friedel oscillations

In this section we expose another characteristic of the Fermi surface by studying the spatial correlations between fermions and antifermions in various mesonic channels, probed via the wavefunction $\Psi(\vec{x})$ defined by

$$\Psi_\Gamma(\vec{x}) = \lim_{x_0 \rightarrow \infty} \Psi_\Gamma^{-1}(\vec{x} = \vec{0}) \sum_{\vec{y}} \langle \mathcal{G}_q(\vec{0}, 0; \vec{y}, x_0) \Gamma \mathcal{G}_{\bar{q}}(\vec{0}, 0; \vec{y} + \vec{x}, x_0) \Gamma \rangle, \quad (5.1)$$

where as usual Γ projects out the quantum numbers of the channel of interest. In the GNM₃ and related models $\Psi(\vec{x})$ is technically much easier to define and measure than in QCD-like theories where they are gauge-dependent. Meson wavefunctions in the $(2+1)d$ GN model have been studied at $T, \mu = 0$ in,¹³⁾ where further technical details are given.

It is easy to show³⁾ that in the large- N_f approximation the PS wavefunction in the chirally broken phase is given by

$$\lim_{x_0 \rightarrow \infty} C(\vec{y}; x_0) \sim \frac{M}{x_0} e^{-2Mx_0} \exp\left(-\frac{|\vec{y}|^2 M}{4x_0}\right). \quad (5.2)$$

The general profile of the wavefunction is a gaussian with width increasing as $\sqrt{x_0}$. In the chirally symmetric phase we get,

$$\lim_{x_0 \rightarrow 0} C(\vec{y}; x_0) \sim \frac{\mu}{x_0} e^{-2\mu x_0} J_0(\mu |\vec{y}|). \quad (5.3)$$

The wavefunction profile no longer changes with x_0 , but instead oscillates with a spatial frequency determined by μ , which to this order may be identified with the Fermi momentum k_F . The oscillations observed in $C(\vec{y}; x_0)$ are characteristic of a sharp Fermi surface and are reminiscent of oscillations in either the density-density correlation function, or the screened inter-particle potential, in degenerate systems generically known as *Friedel Oscillations*.¹⁴⁾ In Fig. 5 we plot the PS wavefunctions

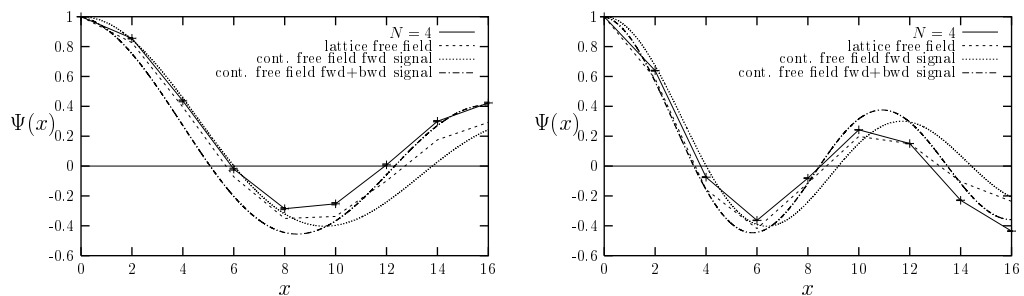


Fig. 5. Scalar wavefunction at $\mu = 0.4$ (left) and $\mu = 0.6$ (right).

at $1/g^2 = 0.75$ for $\mu = 0.4, 0.6$. The simulation data are connected by solid lines. As μ , and hence k_F increases the oscillations decrease in wavelength in accordance with the theoretical expectation and provide a graphic illustration of the presence

of a sharp Fermi surface. The dashed lines show measurements taken with the same lattice parameters but with the interaction switched off. The disparity with the interacting theory is small, though increasing with $|\vec{x}|$, showing that the free field description of the oscillations is qualitatively correct. A possible explanation is the infinite value predicted for the Debye mass in section 3, implying that interactions between static quarks at non-zero $|\vec{x}|$ are completely screened. Also shown is the theoretical form (eq. 5.3) $\Psi(x) = J_0(k_F x)$ with $k_F \equiv \mu$, showing good agreement with the data for small $x \lesssim 2k_F^{-1}$. Unfortunately it appears hard to obtain more quantitative information, such as an independent fit for the Fermi momentum k_F , because $|J_0(kx)|$ decays only as $x^{-\frac{1}{2}}$. This means that fits should not only include the backwards-propagating signal $J_0(k_F(L_s - x))$ but also image contributions $J_0(k_F(nL_s - x))$ – our attempts to find a satisfactory fit were unsuccessful. The figures therefore simply show both the “forwards” $J_0(\mu x)$ and “forwards-and-backwards” $J_0(\mu x) + J_0(\mu(L_s - x))$ forms, showing that neither gives a satisfactory description of the data over the full range of x and μ . We also checked that there are no significant differences among the various mesonic channels, implying that in contrast to the situation at $\mu = 0$,¹³⁾ effects due to eg. σ exchange are very hard to detect.

§6. Summary

The four-fermion models remain the only interacting fermionic field theories both simulable by standard lattice methods at $\mu \neq 0$ and displaying a Fermi surface, thought to be an essential figure of dense quark matter. We have shown that the $\mu \neq 0$, $T = 0$ transition is strongly first order and a tricritical point exists in the (μ, T) plane at very low T .

We also discussed in-medium effects on the character of mesons. The large- N_f auxiliary boson propagator has a branch-cut in the complex- k plane which is modified to an isolated pole in the high density phase. Lattice simulations with $N_f = 4$ have verified this with reasonable precision. We have also shown that the connected (flavor non-singlet) diagrams instead of showing exponential falloff with Euclidean time, they generically decay algebraically, signalling the presence of massless particle-hole excitations. We also presented tentative evidence for a massless pole in the vector channel, which is possibly a manifestation of zero sound. Furthermore, a graphic confirmation of the presence of a sharp Fermi surface was shown by the oscillatory behavior in mesonic wavefunctions, which resemble the Friedel oscillations in many-body physics.

Acknowledgements

The work presented here was done in collaboration with Simon Hands,³⁾ John Kogut^{9),3)} and Thao Tran.³⁾

References

- 1) B. Rosenstein, B.J. Warr and S.H. Park, Phys. Rep. **205** (1991), 59.
- 2) S.J. Hands, A. Kocic and K.B. Kogut, Ann. Phys. **224** (1993), 29.
- 3) S.J. Hands, J.B. Kogut, C.G. Strouthos and T.N. Tran, **D68** (2003), 016005.
- 4) S.J. Hands, B. Lucini and S.E. Morrison, Phys. Rev. **D65** (2002), 036004.
- 5) K.G. Klimenko, Z. Phys. **C37** (1988), 457.
B. Rosenstein, B.J. Warr and S.H. Park, Phys. Rev. **D39** (1989), 3088.
S.J. Hands, A. Kocic and J.B. Kogut, Nucl. Phys. **B390** (1993), 355.
- 6) S. Hands, S. Kim and J.B. Kogut, Nucl. Phys. **B442** (1995), 364.
- 7) M.A. Stephanov, Phys. Rev. Lett. **76** (1996), 4472.
- 8) I. Barbour, S. Hands, J.B. Kogut, M.-P. Lombardo and S. Morrison, Nucl. Phys. **B557** (1999), 327.
- 9) J.B. Kogut and C.G. Strouthos, Phys. Rev. **D63** (2001), 054502.
- 10) M. Buballa, Nucl. Phys. **A609** (1996), 519.
- 11) J.B. Kogut, M.A. Stephanov and C.G. Strouthos, Phys. Rev. **D58** (1998), 096001.
- 12) C.R. Allton, J.E. Clowser, S.J. Hands, J.B. Kogut and C.G. Strouthos, Phys. Rev. **D66** (2002), 094511.
- 13) S.J. Hands, J.B. Kogut and C.G. Strouthos, Phys. Rev. **D65** (2002), 202302.
- 14) A.L. Fetter and J.D. Walecka, *Quantum Theory of Many-Particle Systems*, (McGraw-Hill, New York, 1971).